



# WRF-PDAF v1.0: implementation and application of an online localized ensemble data assimilation framework

Changliang Shao<sup>1,2</sup> and Lars Nerger<sup>2</sup>

<sup>1</sup>China Meteorological Administration Meteorological Observation Centre, Beijing, 100081, China

<sup>2</sup>Alfred-Wegener-Institut, Helmholtz-Zentrum für Polar- und Meeresforschung (AWI), 27570 Bremerhaven, Germany

**Correspondence:** Changliang Shao (shaocl@cma.gov.cn)

Received: 9 October 2023 – Discussion started: 13 November 2023

Revised: 14 March 2024 – Accepted: 7 April 2024 – Published: 29 May 2024

**Abstract.** Data assimilation is a common technique employed to estimate the state and its associated uncertainties in numerical models. Ensemble-based methods are a prevalent choice, although they can be computationally expensive due to the required ensemble integrations. In this study, we enhance the capabilities of the Weather Research and Forecasting–Advanced Research WRF (WRF-ARW) model by coupling it with the Parallel Data Assimilation Framework (PDAF) in a fully online mode. Through minimal modifications to the WRF-ARW model code, we have developed an efficient data assimilation system. This system leverages parallelization and in-memory data transfers between the model and data assimilation processes, greatly reducing the need for file I/O and model restarts during assimilation. We detail the necessary program modifications in this study. One advantage of the resulting assimilation system is a clear separation of concerns between data assimilation method development and model application resulting from PDAF’s model-agnostic structure. To evaluate the assimilation system, we conduct a twin experiment simulating an idealized tropical cyclone. Cycled data assimilation experiments focus on the impact of temperature profiles. The assimilation not only significantly enhances temperature field accuracy but also improves the initial  $U$  and  $V$  fields. The assimilation process introduces only minimal overhead in runtime when compared to the model without data assimilation and exhibits excellent parallel performance. Consequently, the online WRF-PDAF system emerges as an efficient framework for implementing high-resolution mesoscale forecasting and reanalysis.

## 1 Introduction

Data assimilation (DA) plays a pivotal role in enhancing the precision and dependability of numerical weather prediction (NWP) models, effectively bridging the divide between model simulations and real-world observations. It bolsters the accuracy, proficiency, and trustworthiness of weather forecasts, supplying invaluable insights for a diverse array of applications, encompassing weather prediction, climate research, and environmental assessments (Lorenc, 1986; Song et al., 2022).

Based on the mode of data transfer between the numerical model and assimilation algorithm, ensemble-based DA computational setups can be categorized into two coupling modes: offline and online DA. In offline DA, data exchanges between the model ensemble and assimilation algorithm happen through disk files. Examples of this approach encompass the Advanced Regional Prediction System Data Assimilation System (ARPSDAS; Xue et al., 2000), the Data Assimilation Research Testbed (DART; Anderson et al., 2009), the Gridpoint Statistical Interpolation (GSI) ensemble Kalman filter (EnKF) system (Kleist et al., 2009), the Weather Research and Forecasting model’s Community Data Assimilation system (WRFDA; Barker et al., 2012), and WRF-EDAS (Ensemble Data Assimilation System; Zupanski et al., 2011). Offline DA offers convenience for implementing DA procedures in relatively short timeframes. Although the actual I/O time may not be substantial, as described by, e.g., Karspeck et al. (2018), offline DA systems incur costs associated with restarting the model after each analysis cycle for ensemble simulations and the potential redistribution of data.

Online DA is typically implemented by coupling a numerical model and DA algorithm into a single executable program

and exchanging data between the model and assimilation in memory. Notable online DA systems include the ensemble DA system by Zhang et al. (2007) based on the Geophysical Fluid Dynamics Laboratory coupled climate model (CM2) and the ensemble DA system (Sun et al., 2022) based on the Community Earth System Model (CESM). Further, the Parallel Data Assimilation Framework (PDAF, Nerger and Hiller, 2013) provides online DA, e.g., in its implementation with the fully coupled Alfred Wegener Institute Climate Model (AWI-CM; Nerger et al., 2020; Mu et al., 2023). In this paper, PDAF version 2.0 (<http://pdaf.awi.de>, last access: 21 February 2023) is adopted to carry out the coupling work. In this version, the interface for observations, named the Observation Module Infrastructure (OMI), is completely newly developed.

The WRF-ARW model (Skamarock et al., 2021) has gained extensive usage in regional research and real-time forecasting. It is a regional modeling system serving atmospheric research and operational weather prediction communities. Different studies have explored extensive DA works with WRF, such as WRFDA (Wang et al., 2008; Liu et al., 2020), WRF-DART (Kurzrock et al., 2019; Risanto et al., 2021), and WRF-GSI (Yang et al., 2015; Liu et al., 2018). These studies are predominantly grounded in offline DA frameworks, necessitating read and write operations for restart files at each assimilation time step and model restarts for each subsequent forecast phase. This time-intensive approach poses challenges for generating efficient high-resolution reanalysis. In pursuit of an efficient reanalysis, particularly with the goal of high-resolution WRF-ARW DA, an online DA system coupled with WRF-ARW has emerged as an imperative need. This study presents an extension of WRF-ARW's capabilities by introducing the online-coupled WRF-PDAF (Shao, 2023a) DA system to bolster its potential for mesoscale research and high-resolution DA applications. WRF-PDAF facilitates in-memory data transfer, avoiding the need for repeated model restarts and thus enabling efficient support for high-resolution simulations. Further, WRF-PDAF utilizes ensemble parallelization to ensure computational efficiency.

For the application of DA, temperature ( $T$ ) profile observations have gained significant attention in recent years due to their potential for enhancing atmospheric models and weather forecasts. These observations can be derived from various remote sensing instruments, including radiosondes, dropsondes, ground-based and space-based lidars, and microwave radiometers. The assimilation of temperature profiles into atmospheric models using techniques like ensemble Kalman filtering (EnKF) has yielded substantial improvements in model accuracy and performance (Raju et al., 2014), particularly in the realm of short-term forecasts (Rakesh et al., 2009). Such assimilation aids in capturing mesoscale weather phenomena like convective systems, thunderstorms, and localized rainfall patterns. It contributes to the more faithful representation of atmospheric processes, enhancing

the skill of weather forecasts, particularly in regions where traditional observations are sparse or limited (Feng and Pu, 2023). Assimilating profiles facilitates a more precise vertical profiling of atmospheric parameters, critical for comprehending the vertical structure of the atmosphere (Holbach et al., 2023). Real-time assimilation of profiles enables timely updates to atmospheric models, leading to improved nowcasting and short-term forecasts. This real-time assimilation empowers models to capture swiftly evolving atmospheric conditions, providing crucial insights for severe weather events and rapid weather developments (Pena, 2023).

This paper serves as an introduction of the fully online-coupled WRF-PDAF system with a focus on its development and design. Additionally, the study assesses the DA behavior of the system in the case of the assimilation of  $T$  profiles using the ensemble Kalman filtering (EnKF) technique. Twin experiments employing synthetic observations are conducted, and the assimilation results are analyzed, with a specific focus on fully online assimilation of  $T$  profiles.

The subsequent sections of this study are organized as follows: Sect. 2 provides an overview of the WRF model and its configuration, the tropical cyclone case, the twin experiments, and the ensemble filtering algorithm. Section 3 details the implementation of the ensemble-based online WRF-PDAF DA system, including descriptions of the PDAF system (Sect. 3.1), the augmentation of WRF for DA with PDAF (Sect. 3.2), and discussions on interfaces for model fields and observations (Sect. 3.3). Section 4 encompasses the assessment of the scalability and an evaluation of the assimilation behavior with the online WRF-PDAF system. Finally, Sect. 5 offers a summary and discusses the findings.

## 2 Methodology

In this section, we introduce the WRF model and its configuration, the tropical cyclone case, the local ensemble square root transform Kalman filter (LESTKF) assimilation scheme, and the twin experiment.

### 2.1 WRF

The WRF model stands as a widely embraced numerical weather prediction system, offering a versatile platform for simulating a broad spectrum of atmospheric processes. Its applicability spans both regional and global weather simulations, all thanks to its modular structure, enabling tailoring to specific research goals or operational forecasting requirements. The dependability and flexibility inherent in WRF make it an invaluable tool for our study. In this work, we harnessed WRF-ARW version 4.4.1.

In this study, we have adopted the idealized tropical cyclone case provided by WRF as our test case. Tropical cyclones represent formidable and destructive meteorological

phenomena originating over warm ocean waters near the Equator. These potent storms draw their energy from the latent heat release accompanying the ascent and condensation of moist air into clouds and precipitation. The idealized tropical cyclone case offers a controlled environment for conducting identical twin experiments, evaluating system scalability, and assessing the behavior of DA with WRF-PDAF. The simulation domain encompasses  $3000 \text{ km} \times 3000 \text{ km} \times 25 \text{ km}$ , comprising  $200 \times 200 \times 20$  grid points with a horizontal grid spacing of 15 km and a vertical grid spacing of 1.25 km. The simulation spans a period of 6 d, commencing on 1 September at 00:00 UTC (010000) and concluding on 7 September at 00:00 UTC (070000). The model employs a time step of 60 s, the Kessler microphysics scheme, and the YSU (Yonsei University) boundary layer physics, with radiation schemes omitted. The initialization of the simulation necessitates both initial and boundary conditions. The initial state establishes a horizontally homogeneous environment defined via the default file employing the Jordan mean hurricane sounding, named “input\_sounding” within the WRF directory. The initial state is characterized by immobility ( $u = v = 0$ ) and horizontally homogeneity, with the addition of an analytical axisymmetric vortex in hydrostatic and gradient–wind equilibrium. Additionally, periodic lateral boundary conditions are imposed to facilitate the simulation process.

## 2.2 LESTKF

The EnKF technique serves as a data assimilation method, amalgamating information from a model state ensemble and observational data to refine the model state variables. EnKFs use an initial state ensemble created by introducing perturbations to the model initial conditions. Subsequently, assimilation updates are performed by estimating analysis increments, taking into account both the ensemble spread and the misfit between observations and model predictions. In this context, ensemble spread, quantified as the ensemble standard deviation (SD), characterizes the dispersion of the ensemble members around the ensemble mean. The analysis increments derived from this process are then applied to the ensemble members, resulting in updated state variables. The EnKF encompassed various variants suitable for assimilating  $T$  profiles due to their capacity to manage the nonlinear dynamics typical of atmospheric models. Examples of such variants include the local ensemble transform Kalman filter (Hunt et al., 2007; LETKF) and the local error-subspace transform Kalman filter (Nerger et al., 2012; LESTKF).

The LESTKF has found application across diverse studies, encompassing the assimilation of satellite data into atmosphere models (Mingari et al., 2022), ocean models (Goodliff et al., 2019), atmosphere–ocean coupled models (Nerger et al., 2020; Zheng et al., 2020), and hydrological models (Y. Li et al., 2023). In the context of the LESTKF, the EnKF procedure is efficiently formulated, facilitating discussion on the unique aspects of DA with respect to the ensemble filter.

In the mathematical framework, each state vector comprises model fields transformed into a one-dimensional vector, represented as  $\mathbf{x}^f$ . The columns of the forecast ensemble matrix  $\mathbf{X}^f$  hold the  $N_e$  state vectors.  $\mathbf{y}$  represents observation vector. As we are aware, temperature serves as a common state variable. It is intelligible to assimilate  $T$  profiles, thereby assessing the efficiency and performance of the framework. The analysis in Eqs. (1)–(4) facilitates the transformation of the forecast ensemble  $\mathbf{X}^f$  of  $N_e$  model states into the analysis ensemble  $\mathbf{X}^a$ .

$$\mathbf{X}^a = \mathbf{X}^f \left( \mathbf{w} \mathbf{1}_{N_e}^T + \tilde{\mathbf{W}} \right) + \bar{\mathbf{x}}^f \mathbf{1}_{N_e}^T \quad (1)$$

$$\mathbf{w} = \mathbf{M} \mathbf{A} \left( \mathbf{H} \mathbf{X}^f \mathbf{T} \right)^T \mathbf{R}^{-1} (\mathbf{y} - \mathbf{H} \bar{\mathbf{x}}^f) \quad (2)$$

$$\tilde{\mathbf{W}} = \sqrt{N_e - 1} \mathbf{M} \mathbf{A}^{1/2} \mathbf{M}^T \quad (3)$$

$$\mathbf{A}^{-1} = \alpha (N_e - 1) \mathbf{I} + \left( \mathbf{H} \mathbf{X}^f \mathbf{M} \right)^T \mathbf{R}^{-1} \mathbf{H} \mathbf{X}^f \mathbf{M} \quad (4)$$

Here,  $\bar{\mathbf{x}}^f$  represents the ensemble mean state of the forecast, and  $\mathbf{1}_{N_e}^T$  is the transpose of a vector of size  $N_e$ , containing the value 1 in all elements. The vector  $\mathbf{w}$  with a size of  $N_e$  facilitates the transformation of the ensemble mean from the forecast to the analysis, while the matrix  $\tilde{\mathbf{W}}$  (size  $N_e \times N_e$ ) manages the transformation of ensemble perturbations. The matrix  $\mathbf{M}$  defined by Eq. (5) projects into the error subspace.  $\mathbf{H}$  is the observation operator.  $\mathbf{R}$  is the observation error covariance matrix.  $\mathbf{A}$  is a transform matrix in the error subspace.  $\alpha$  is the forgetting factor (Pham et al., 1998) used to inflate the ensemble to avoid underestimation of the forecast uncertainty. It leads to an inflation of the ensemble variance by  $1/\alpha$ .

The forecast ensemble represents an error subspace of dimension  $N_e - 1$ , and the ensemble transformation matrix and vector are computed in this subspace. Practically, one computes an error-subspace matrix by  $\mathbf{L} = \mathbf{X}^f \mathbf{M}$ , where  $\mathbf{M}$  is a matrix with  $j = N_e$  rows and  $i = N_e - 1$  columns that is defined by the following.

$$\mathbf{M}_{j,i} = \begin{cases} 1 - \frac{1}{N_e} \frac{1}{\frac{1}{\sqrt{N_e}} + 1} & \text{for } i = j, j < N_e \\ -\frac{1}{N_e} \frac{1}{\frac{1}{\sqrt{N_e}} + 1} & \text{for } i \neq j, j < N_e \\ -\frac{1}{\sqrt{N_e}} & \text{for } i = N_e \end{cases} \quad (5)$$

The matrix  $\mathbf{A}^{1/2}$  in Eq. (3) is computed using the eigenvalue decomposition of  $\mathbf{A}^{-1}$ , calculated as

$$\mathbf{U} \mathbf{S} \mathbf{U}^T = \mathbf{A}^{-1}, \quad (6)$$

where  $\mathbf{U}$  and  $\mathbf{S}$  denote the matrices of eigenvectors and eigenvalues. Consequently,  $\mathbf{A}$  in Eq. (2) is computed as

$$\mathbf{A} = \mathbf{U} \mathbf{S}^{-1} \mathbf{U}^T. \quad (7)$$

Similarly, the symmetric square root  $\mathbf{A}^{1/2}$  in Eq. (3) is computed as follows.

$$\mathbf{A}^{1/2} = \mathbf{U} \mathbf{S}^{-1/2} \mathbf{U}^T \quad (8)$$

If  $\mathbf{A}^{-1}$  is rank-deficient, the calculations in Eqs. (6) and (7) can be performed only for the nonzero eigenvalues. Each grid point in the model is independently updated through a local analysis step. Only observations falling within specified horizontal and vertical localization radii are considered during grid point updates. Therefore, the observation operator is localized and computes an observation vector within these localization radii. Furthermore, each observation is weighted based on its distance to the grid point (Hunt et al., 2007), and a fifth-order polynomial function with a Gaussian-like shape, following the Gaspari and Cohn (1999) approach, is employed to determine these weights. The localization weights are applied to modify the matrix  $\mathbf{R}^{-1}$  in Eqs. (2) and (4). As a result, the localization process yields individual transformation weights  $\mathbf{w}$  and  $\tilde{\mathbf{W}}$  for each local analysis domain. Like the LETKF, the LESTKF performs a sequence of local analyses. However, it does the calculations directly in the error subspaces spanned by the ensemble. This can lead to computational savings compared to the LETKF.

### 2.3 DA twin experiments

Table 1 provides an overview of the experiments conducted in this study. The setups for the true state (Exp. 1, “True”), the control state (Exp. 2, “CTRL”), and the free ensemble run (Exp. 3, “ENS”) are consistent with Shao and Nerger (2024). The CTRL is derived from a single free run, which mirrors the True in all aspects, except for a 60 h delay in its starting time. The ENS, comprising 40 ensemble members, is generated by introducing an initial perturbation to the CTRL. According to the ENS, the DA twin experiments are implemented by assimilating observations using different localization radii. Hourly synthetic observations of  $T$  profiles are generated from the true state on a span of 30 h, starting from 040800 and ending at 051400. The observations are located on all of the model grid points, so the  $T$  profiles have the same resolution as the model grid. Actually, values on all model levels are used to generate profiles. However, random Gaussian noise is also added to the model value. To this end, the assumption of observation errors being uncorrelated is still valid. Assimilation experiments (Exps. 4–14, “ANA(0–10)”) are carried out based on the ensemble run using observations from  $T$  profiles over 30 analysis cycles. These experiments vary in terms of horizontal localization radii, ranging from 0 to 10 times the horizontal grid spacing ( $dx$ ), where  $dx$  is 15 km. The vertical localization radii are identical, matching the height of the model top. The impact of assimilating  $T$  profile observations on the model representation of  $T$ , as well as the horizontal velocities  $U$  and  $V$ , is assessed by comparing the assimilated states with the true states. These experiments allow us to evaluate the performance and effectiveness of WRF-PDAF in assimilating observations and improving the model representation of atmospheric variables.

In these twin experiments, synthetic observations are generated directly at the model grid points so that no interpola-

**Table 1.** The design for varying the localization radius ( $dx = 15$  km).

Exp.	Name	Member (s)	DA cycle (s)	Localization radius (km)
1	True	1	–	–
2	CTRL	1	–	–
3	ENS	40	–	–
4–14	ANA(0–10)	40	30	0–10 $dx$

tions are required. Thus, the observation operator for profile data simply selects the  $T$  values at the model grid points. Gaussian noise, with a standard deviation of 1.2 K following L. Li et al. (2023), is added to the  $T$  field of the True run to generate the observations. Each profile represents a single vertical column of observations located at grid points. These profile data are then assimilated into the WRF model using the LESTKF. The twin experiments commence at 031200, undergoing a spin-up period of 20 h. Following this, observations are assimilated hourly during the analysis period, spanning from 040800 to 051400. Subsequently, an ensemble forecast is executed without additional assimilation from 051400 until 070000. To apply ensemble inflation, a forgetting factor  $\alpha$ , where  $0 < \alpha \leq 1$ , is employed. In this study, an adaptive scheme for the forgetting factor is adopted, utilizing the statistical consistency measures outlined by Desroziers et al. (2005), analogous to Brusdal et al. (2003).

## 3 Setup of the data assimilation program

The process of coupling the WRF with the PDAF involves integrating function calls from PDAF into the WRF model code to enable data assimilation capabilities. This section provides an overview of the assimilation framework and the setup of the DA program. Firstly, a summary of the PDAF is presented in Sect. 3.1. The modifications made to enable online coupling are explained in Sect. 3.2. Furthermore, Sect. 3.3 discusses the implementation of the interfaces for model fields and observation.

### 3.1 Description of PDAF

PDAF is open-source software designed to simplify the implementation and application of ensemble and variational DA methods. It provides a modular and generic framework, including fully implemented and parallelized ensemble filter algorithms like LETKF, LESTKF, NETF (Tödter and Ahrens, 2015), and LKNETF (Nerger, 2022), along with related smoothers and variational methods like 3D-Var or 3D-EnVar following Bannister (2017). PDAF also handles model parallelization for parallel ensemble forecasts and manages the communication between the model and DA codes. Written in Fortran, PDAF is parallelized using the Message Passing Interface (MPI) standard (Gropp et al., 1994) and

OpenMP (Chandra et al., 2001; OpenMP, 2008), ensuring compatibility with geoscientific simulation models. However, PDAF can still be used with models implemented in other programming languages such as C and Python.

The filter methods within PDAF are model-agnostic and exclusively operate on abstract state vectors, as detailed in Sect. 2.3 for LESTKF. This design promotes the development of DA techniques independently from the underlying model and simplifies the transition between different assimilation approaches. Model-specific tasks, such as those concerning model fields, the model grid, or assimilated observations, are executed through user-provided program routines based on existing template routines. These routines are equipped with specified interfaces and are invoked by PDAF as call-back routines. Thus, the model code executes PDAF routines, which in turn call the user routines. To streamline these interactions, calls to PDAF are integrated into interface routines. These routines define the parameters for invoking the PDAF library routines before the actual PDAF routine is executed. Consequently, this approach minimizes changes required within the model code itself, as it mandates only a single-line call to each interface routine – a total of three routines. This call structure presents the advantage of enabling the call-back routines to exist within the context of the model, thus allowing them to be implemented in a manner akin to model routines. Additionally, the call-back routines can access static arrays allocated by the model, such as through Fortran modules or C header files. This capability facilitates the retrieval of arrays storing, e.g., model fields or grid information, exemplifying the versatility of the system.

### 3.2 Augmenting WRF for DA with PDAF

We adopt a fully online coupling strategy for DA here. This approach assumes the availability of an adequate number of processes to support concurrent time stepping of all ensemble states, thereby simplifying the implementation. Each ensemble state is integrated by one model task, which can encompass several processes to, e.g., allow for domain decomposition. This approach allows each model task to consistently progress forward in time. While the general strategy for online coupling of DA remains consistent with prior studies (Nerger and Hiller, 2013; Nerger et al., 2020; Mu et al., 2023), we present a comprehensive description here to illustrate the implementation of the coupling process for the WRF model. The augmentation of WRF with DA functionality can be visualized as depicted in Fig. 1.

In Fig. 1, solid boxes delineate the typical flow of the WRF model flow. The program initiates in WRF\_INIT, initializing parallelization, followed by activating all relevant processes. Subsequently, the model is initialized, incorporating grid configuration and initial fields retrieval from files. After completing model initialization, the time-stepping process commences in the routine INTEGRATE. Following time

stepping, WRF undergoes cleanup in WRF\_FINALIZE, finalizing parallelization and concluding the program.

Dashed boxes signify essential additions to the model code for online coupling with PDAF. These additions involve subroutine calls that serve as interfaces between the model code and the DA framework. By incorporating these subroutine calls, the DA functionality seamlessly integrates into the WRF code, allowing WRF to utilize the DA algorithms. Typically, these subroutine calls entail single-line additions and can be enclosed in preprocessor checks to enable users to activate or deactivate the data assimilation extension during compilation.

The general functionality of the inserted routines is analogous to their roles in a coupled model system (Nerger et al., 2020) as follows.

- *Init\_parallel\_pdaf*. This routine is merged into the initialization phase to commence parallelization and modify the model parallelization for running an ensemble of model tasks. The parallelization of WRF adheres to the MPI standard. It is initialized at the outset of the program, generating the MPI\_COMM\_WORLD communicator that encompasses all program processes. Domain decomposition is employed, with each process computing a designated region within the global domain. For ensemble DA, *init\_parallel\_pdaf* adapts the parallelization to accommodate the concurrent computation of multiple model tasks. Achieving this entails partitioning the MPI\_COMM\_WORLD communicator into communicators for WRF model tasks, termed COMM\_model, each with the same number of processes as used by the original domain decomposition. Each communicator within COMM\_model represents a distinct model task within the ensemble. To enable this MPI\_COMM\_WORLD partitioning, the source code of WRF was modified by substituting MPI\_COMM\_WORLD with COMM\_model. In the case of a single model task, COMM\_model would be equal to MPI\_COMM\_WORLD. In addition to COMM\_model, two more communicators are defined for the analysis step in PDAF. COMM\_couple facilitates coupling between WRF and PDAF, while COMM\_filter encompasses all processes involved in the initial model task. PDAF provides a template for *init\_parallel\_pdaf*, which users can customize as per specific requirements.
- *Init\_pdaf*. Inserted just before the time-stepping loop in the model code, this routine initializes the PDAF framework. It specifies parameters for the DA, which may be read from a configuration file or provided via command line inputs. Subsequently, the initialization routine for PDAF is invoked, configuring the PDAF framework and allocating internal arrays, including the ensemble state array. At this juncture, the initial ensemble is initialized. This can be performed using second-order exact sam-

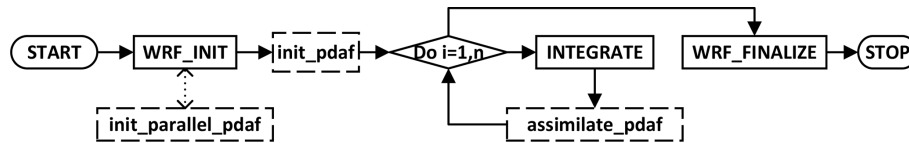


**Figure 1.** General program flow of WRF-PDAF. Solid boxes indicate routines in WRF that require parallelization adjustments for data assimilation. Dashed boxes represent essential additions to the model code. Solid lines represent flow, while the dotted line marks a function call inside a routine.  $n$  represents the total number of time steps.

pling (Pham et al., 1998) from a decomposed covariance matrix. For this, a call-back routine, `init_ens_pdaf`, is called to read the covariance matrix information and generate the initial ensemble. Once PDAF is initialized, information from the initial ensemble is written into the model's field arrays. Subsequently, the initial forecast phase is initialized, entailing a specific number of time steps until the initial analysis step.

- *Assimilate\_pdaf*. This routine is invoked at the conclusion of each model time step. It calls a filter-specific PDAF routine responsible for computing the analysis step of the selected filter method. Before executing the analysis step, the PDAF routine verifies whether all time steps of a forecast phase have been computed. The analysis step includes additional operations such as handling observations, as further described below.

### 3.3 Interfaces for model fields and observation

PDAF interfaces play a pivotal role in executing model- and observation-specific operations, designed to maintain low complexity. Two types of interfaces are introduced: those for model fields and those for observations.

#### 3.3.1 Interface for model fields

This interface encompasses two key routines: `collect_state_pdaf` and `distribute_state_pdaf`. These routines are invoked before and after the analysis step, respectively, to facilitate the exchange of information between the WRF model fields and the state vector of PDAF. The routine `collect_state_pdaf` transfers data from the model fields to the state vector, while `distribute_state_pdaf` initializes the model fields based on the state vector. Both routines execute across all processes involved in model integrations, each operating within its specific process subdomain. The variables of WRF essential for PDAF are the wind components ( $u, v, w$ ,  $\text{m s}^{-1}$ ), perturbation geopotential ( $ph$ ,  $\text{m}^2 \text{s}^{-1}$ ), perturbation potential temperature ( $th$ , K), water vapor mixing ratio ( $qv$ ,  $\text{kg kg}^{-1}$ ), cloud water mixing ratio ( $qc$ ,  $\text{kg kg}^{-1}$ ), rain water mixing ratio ( $qr$ ,  $\text{kg kg}^{-1}$ ), ice mixing ratio ( $qi$ ,  $\text{kg kg}^{-1}$ ), snow mixing ratio ( $qs$ ,  $\text{kg kg}^{-1}$ ), graupel mixing ratio ( $qg$ ,  $\text{kg kg}^{-1}$ ), perturbation pressure ( $p$ , Pa), density ( $\rho$ ,  $\text{kg m}^{-3}$ ), and base-state geopotential ( $phb$ ,  $\text{m}^2 \text{s}^{-1}$ ). Note that some of these variables, namely  $p$ ,  $\rho$ , and  $phb$ , are exclusively used by the

observation operators and remain unaltered by PDAF. Consequently, only the remaining variables are updated and written back to WRF.

Additionally, there is a routine called `prepoststep_pdaf` that permits users to access the ensemble both before and after the analysis step. This functionality enables pre- and post-processing tasks, such as calculating the ensemble mean, which can be saved to a file. Users can also perform consistency checks, ensuring that variables like hydrological properties remain physically meaningful, and make necessary corrections to state variables if required.

In cases when the analysis step incorporates localization, which is typically the case in high-dimensional models like WRF, additional routines are invoked to handle the localization of the state vector. Initially, these routines ascertain the coordinates and dimension of the local state vector for a given index within a local analysis domain. In WRF-PDAF the local analysis domain is chosen to be a single grid point, in contrast to the implementation in AWI-CM-PDAF (Nerger et al., 2020), which utilizes a vertical column of the model grid as the local analysis domain. Since the local analysis domain is a single grid point here, the dimension of the local state vector is the number of model fields included in the state vector. The other localization functionality is the initialization of a local state vector from the global state vector according to the index of the local analysis domain. Analogously, the global state vector has to be updated from the local state vector after this has been updated by the local analysis.

#### 3.3.2 Interface for observations – Observation Module Infrastructure (OMI)

The implementation utilizes the Observation Module Infrastructure (OMI), a recent extension of PDAF. OMI offers a modular approach to handling observations. In comparison to the traditional approach of incorporating observations with PDAF, OMI presents two notable advantages. The first is simplified implementation: OMI considerably reduces the coding effort required to support various observation types, their respective observation operators, and localization. By defining standards regarding how to initialize observation information, OMI simplifies the process and minimizes the coding complexities associated with handling observations. With this, several routines that had to be coded by the user in

the traditional approach are now handled internally by OMI. The second is enhanced flexibility: OMI enhances flexibility by encapsulating information about each observation type. This encapsulation prevents interference between different observation types. From the code structure, OMI is motivated by object-oriented programming, but for the sake of simplicity, the actual abstraction of object-oriented code is avoided.

Figure 2 provides a visual representation of these interfaces. The interfaces in the OMI framework encompass three key components.

- *Observation initialization.* For each observation type, a dedicated routine reads observations of that type from a file. Then, it tallies the valid observations, accounting for factors like observation quality flags. OMI also provides some features relating to quality control. For example, an observation can be excluded if its value deviates too much from the ensemble mean. The routine initializes the observation coordinates and observation errors. Additionally, it determines which elements of the state vector are required for the observation operator to compute the model counterpart to an observation. If interpolation is involved in the observation operator, interpolation coefficients may be calculated. Once these quantities are initialized, an OMI routine is called, transferring the observation information to OMI for use in the PDAF analysis step. In the twin experiments, observation initialization can generate and read synthetic observations.
- *Observation operator.* This routine, as described in Sect. 2.2, implements the observation operator. It takes an ensemble state vector as input and returns the corresponding observed state vector. This operation is performed for each state vector within the ensemble. The information specifying which elements of the state vector are used in the observation operator and any applicable interpolation weights was initialized by the observation initialization routine. OMI provides some universal operators for interpolations in one, two, and three dimensions, including support for triangular grids. The observation operator with interpolation is generic. One just needs to determine interpolation weights and the indices of the elements in the state vector which are combined. For instance, for profile data, the operator for  $T$  should be implemented in `obs_SOUND_pdafomi`. Furthermore, for complicated remote sensing observation operators, some possible additions would also be implemented. Currently, two operator modules have been implemented, covering sounding observation operators, including  $U$ ,  $V$ , and  $T$ , as well as Global Navigation Satellite System (GNSS) observation operators, including precipitable water (PW) and zenith total delay (ZTD).

- *Observation localization.* The localized analysis, described in Sect. 2.2, necessitates determining the observations within a specified distance around a local analysis domain. For each observation type, a dedicated routine calls an OMI routine to identify these observations by calculating the distance between the local analysis domain and observations based on their coordinates. The OMI routine takes as input a localization radius and the coordinates of the local analysis domain. Internally, OMI performs distance-dependent weighting of observations based on their coordinates. In WRF-PDAF, the local analysis domain consists of a single grid point; hence, the observation localization operates in three dimensions, requiring both horizontal and vertical localization radii to be specified. This contrasts with the observation localization in two dimensions and the use of only horizontal localization radius in AWI-CM-PDAF (Nerger et al., 2020). For satellite observations, the relevant coordinates used for distance calculation are defined by the user.

This structured approach to model fields and observations, as facilitated by PDAF and OMI, ensures a robust and versatile framework for data assimilation within WRF and other geoscientific models. PDAF provides a model-agnostic framework to create an efficient data assimilation system as well as filter and smoother algorithms. As such, it ensures a clear separation of concerns between model development, observations, and assimilation algorithms.

## 4 Evaluation of WRF-PDAF

In this section, we delve into the application of WRF-PDAF, specifically focusing on its utility in DA. We particularly aim for evaluating both the parallel performance and the behavior of DA of  $T$  profiles.

### 4.1 Compute performance

For evaluation of the performance of WRF-PDAF we use an ensemble of 40 tasks, in which each single WRF task is distributed across a total of 64 processes. As a result, we utilize a grand total of 2560 processes for the ensemble DA.  $T$  profiles are placed at 10-grid-point intervals in both the  $x$  and  $y$  directions. In Fig. 3a, we provide a chart outlining execution times of the various steps of the assimilation procedure.

The breakdown of the key execution times for different phases of the assimilation process over the full experiment is as follows: the major execution time of roughly 288.6 s is needed to conduct the ensemble forecasts over 85 h. This time requirement is followed by the communication related to DA coupling (within the communicator `COMM_couple`), encompassing both data collection and distribution within the ensemble, which takes approximately 27.4 s. The initialization stage (in `init_ens_pdaf`), which involves generating

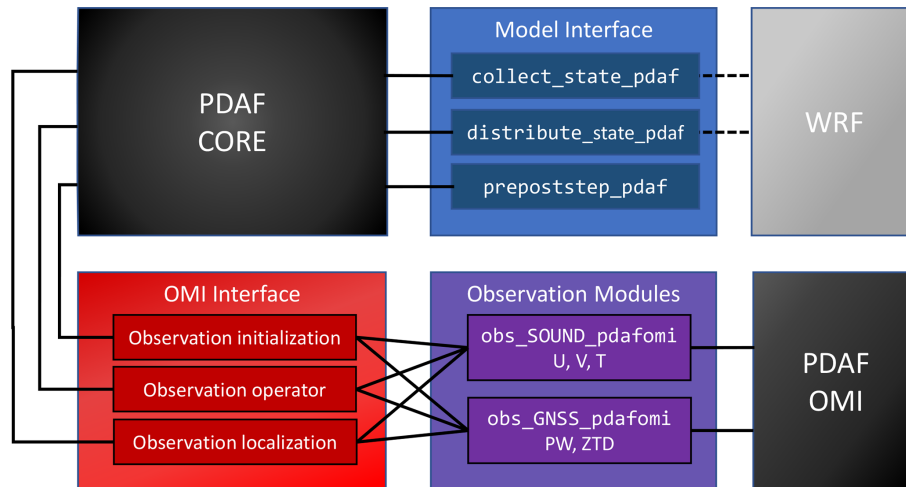


**Figure 2.** Sketch of interfaces for model fields and observation (OMI) in the analysis step. The PDAF core invokes the model interface routines and the OMI interface. The routines `collect_state_pdaf` and `distribute_state_pdaf` incorporate information on the model fields from WRF.

the ensemble, consumes approximately 18.9 s. Less time is spent for the DA analysis, involving 30 cycles in the full experiment, which has a total execution time of 7.4 s. Activities associated with DA pre- and post-processing (in `prepoststep_pdaf`) occupy a combined execution time of 6.6 s.

The time for the DA analysis can be further broken down into three components: PDAF internal operations, observation handling, and variable transformation. Here, the observation handling requires the most time with around 4.9 s. The PDAF internal operations of the LESTKF, like the singular value decomposition and the multiplication of the forecast ensemble with the weight matrix and vector ESTKF, demand approximately 1.9 s. For variable transformation, an additional 0.6 s is dedicated to the transformation of variables between the global and local domains. Overall, the execution time for the entire assimilation process, amounting to 349 s, is largely dominated by the time required for computing forecasts. For individual cycles, the execution times are distributed as follows: 3.4 s for forecasts, 0.9 s for coupling communication, 0.2 s for DA analysis, and 0.2 s for pre- and post-operations, as demonstrated in Fig. 3b. It is crucial to acknowledge that the execution times can vary depending on the distribution of the program across the computing resources. Nevertheless, repeated experiments have consistently shown that the timings depicted in Fig. 3b are representative of the typical performance.

The numerical experiments, with hourly assimilation of  $T$  profiles into WRF, exhibit high efficiency. This efficiency is underscored by an overhead of only up to 20.9 % in computing time when compared to the model without assimilation functionality, with an ensemble size of 40. This favorable outcome is largely attributed to the optimization of the ensemble DA program, which prioritizes efficient ensemble integrations between observations, thus reducing the need for

disk operations. Instead, ensemble information is retained in memory and efficiently exchanged through parallel communication during program runtime. The execution time of the DA analysis is influenced by the number of assimilated observations and will increase if more observations are assimilated.

It is important to highlight that the forecasts presented here are derived from an idealized case, characterized by numerous simplifications. For instance, radiation schemes have been omitted in this idealized scenario, resulting in shorter simulation runtimes compared to real cases. In actual operational scenarios, the model physics would likely be more complex and forecasting times would be notably longer than those in the idealized case. Consequently, when evaluating efficiency by dividing the time dedicated to analysis by that of the forecast, the efficiency values tend to become even more favorable in favor of the assimilation process.

## 4.2 Assimilation results

To assess the influence of the  $T$  profiles, they are assimilated here at all vertical columns. Figure 4 presents the root mean square error (RMSE) over time and the time-averaged (from the start to the end) vertical RMSE profiles for  $T$  and the two horizontal velocity fields  $U$  and  $V$ . The primary focus of the experiments is to evaluate the impact of the horizontal localization radius. Notably, the RMSE of the ensemble forecast (ENS) is lower than that of the control run (CTRL) compared to the true state (True). This suggests that the ensemble approach itself improves the accuracy of the model prediction. Furthermore, when assimilating  $T$  data, the RMSE of  $T$  (Fig. 3) is much lower than that of ENS during the analysis period. Thus, the assimilation process significantly enhances the accuracy of the model prediction. Among the ex-



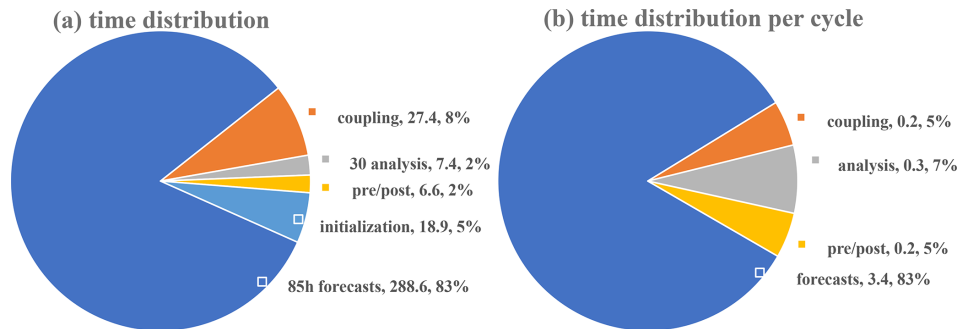


**Figure 3.** Flowchart and execution times for different phases of the DA experiment (unit: s).

periments ANA3, ANA4, and ANA5, there are similarities in RMSE values, with ANA4 exhibiting the lowest RMSE among all the experiments in Table 1. Compared to ANA4, either smaller or larger localization radii lead to increased RMSE. When the assimilation is stopped, the RMSE value increases significantly. At the end of the experiment after 34 h of free forecast, the RMSE for  $T$  from the ANA experiments is at a similar level as the RMSE of ENS.

With the aid of flow-dependent cross-variable background error covariances, the multivariate assimilation of  $T$  profiles not only reduces the errors of the  $T$  field but also leads to improvements in the  $U$  and  $V$  fields. Specifically, in Fig. 4, the RMSEs for  $U$  from the experiments ANA4, ANA5, and ANA6 appear quite similar, with ANA5 exhibiting the lowest RMSE among all the experiments. In Fig. 4, a similar pattern is observed for  $V$ , with ANA4 having the lowest RMSE among all the experiments. This demonstrates that the assimilation of  $T$  data contributes to reduced forecast errors and more consistent forecasts. Note that the localization radius notably influences the assimilation result. An appropriately chosen localization radius leads to improvements in the background model. However, when the localization radius is set to 0, the RMSEs of  $U$  and  $V$  from ANA0 become higher than those from ENS during the forecast period, as shown in Fig. 4b and c. Additionally, after the final assimilation cycle at 051400, the RMSE of  $T$  from ANA0 sharply increases at the first forecast step of 051500, as is visible in Fig. 4. These special behaviors are due to the phenomenon of overfitting; i.e., the model is adjusted not only to the data but also to the noise (Nerger et al., 2006). In contrast the cases ANA1 to ANA10 show a lower RMSE for  $U$  and  $V$  at the end of the experiment. Thus, the assimilation improves the velocity field and some of the improvement remains present in the ensemble also after 34 h of free forecast.

In the time-averaged RMSE profiles, improvements induced by the assimilation are visible in all levels of the model. They are lowest at the uppermost layers.

Figure 5 illustrates the relationship between the localization radius and the RMSEs of  $T$ ,  $U$ , and  $V$ . To achieve the smallest RMSEs, a localization radius of  $4 dx$  is a desirable selection when assimilating the full set of observations. How-

ever, short localization radii ( $< 4 dx$ ) are detrimental to balance. Conversely, long localization radii ( $> 4 dx$ ), when compared to the optimal radius, may lead to larger errors and imbalances due to presumed spurious correlations, aligning with findings by Greybush et al. (2011). It is important to emphasize that the experiments conducted based on different localization radii serve as fundamental demonstrations of the functionality of the DA program, with in-depth analysis not being the primary focus of this study. In addition, the optimal selection is case-dependent. For reference, previous research (Wang and Qiao, 2022; Huang et al., 2021) has discussed the relationship between the observation radius and the background error covariance.

## 5 Discussion and conclusions

This paper introduces and evaluates WRF-PDAF, a fully online-coupled ensemble DA system that couples the atmosphere model WRF with the data assimilation framework PDAF. In comparison to AWI-CM-PDAF 1.0 (Nerger et al., 2020), several key distinctions stand out. Firstly, the coupled models diverge significantly. AWI-CM represents a climate model, whereas WRF is an atmospheric regional model. Consequently, the framework, state vector definition, and incorporated observations are fundamentally dissimilar. Secondly, the PDAF version varies. Notably, the introduction of the newly developed OMI has led to a divergence in code structure. This marks the inaugural use of OMI in implementing observation interfaces. Lastly, there are disparities in computational performance and assimilation outcomes. Importantly, this novel endeavor underscores the adaptability of PDAF, as it proves its efficacy not only in large-scale climate system models but also in mesoscale regional atmospheric models.

A key advantage of the WRF-PDAF configuration is its ability to concurrently integrate all ensemble states, eliminating the need for time-consuming distribution and collection of ensembles during the coupling communication. Figure 6 describes how the ensemble runs and how the PDAF obtains data from the ensemble in online mode. This innovative on-

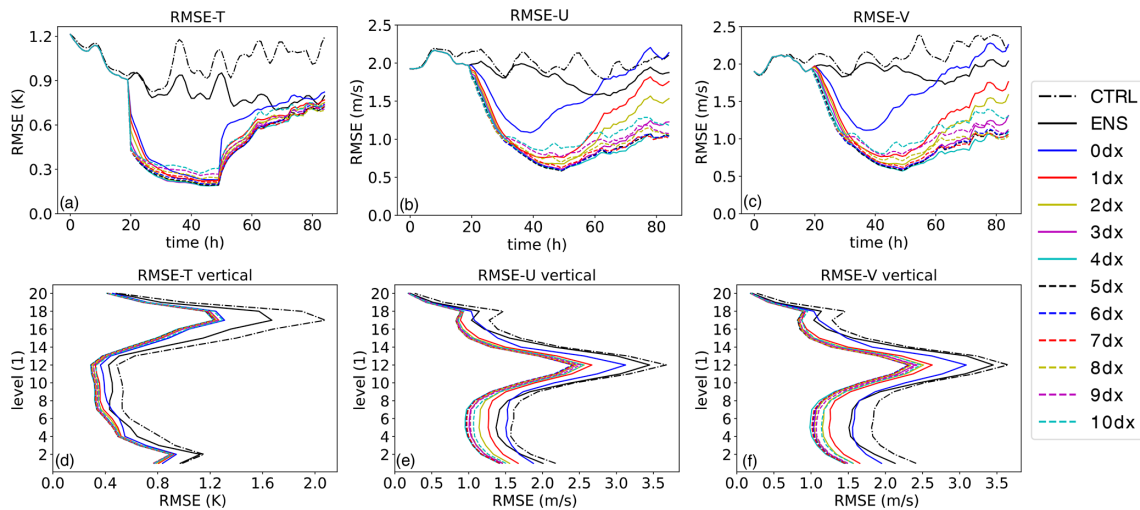


**Figure 4.** The RMSEs of  $T$ ,  $U$ , and  $V$  from 031200 to 070000. **(a)** RMSE of  $T$  in time series; **(b)** RMSE of  $U$ ; **(c)** RMSE of  $V$  in time series; **(d)** vertical average of  $T$  RMSE; **(e)** vertical average of  $U$  RMSE; **(f)** vertical average of  $V$  RMSE.

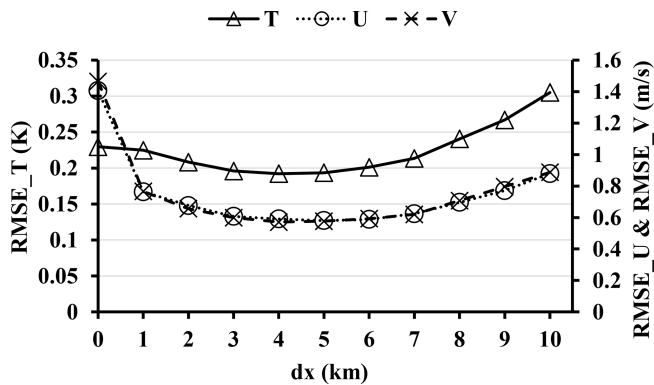


**Figure 5.** The RMSEs of  $T$ ,  $U$ , and  $V$  using different localization radii.

line DA system eliminates the necessity for frequent model restarts, a common requirement in offline DA systems. Without the need for model restarts and file I/O operations, the extra time required for DA, including the analysis, communication, and pre- and post-operations, amounts to only 20.6 % per cycle in our test assimilation of  $T$  profile observations every hour for 30 cycles. Twin experiments focusing on an idealized tropical cyclone configuration were conducted to validate that the WRF-PDAF system works correctly. The results underscore the effectiveness of the WRF-PDAF system in assimilating  $T$  profile data, leading to significant enhancements not only in three-dimensional temperature fields but also in three-dimensional wind components ( $U$  and  $V$ ). The choice of an optimal localization radius is demonstrated, although it is important to note that the localization distance can vary depending on the specific case.

The code structure using interface routines inserted into the WRF model code and observation-specific OMI routines

make the assimilation framework highly flexible. Further, the abstraction in the analysis step, which uses only state and observation vectors without accounting for the physical fields, allows one to separate the development of advanced DA algorithms from the development of the model. Therefore, ensuring a clear separation of concerns becomes imperative, a requirement for the efficient development of intricate model codes and their adaptation to contemporary computing systems (Lawrence et al., 2018). The separation allows all users with their variety of models to use newly implemented DA methods by updating the PDAF library and, if the new method has additional parameters, to specify the additional DA. To guarantee compatibility across various library versions, the interfaces to the PDAF routines remain unaltered. The abstraction in the analysis step and the model-agnostic code structure also allow users to apply the assimilation framework independently of the specific research domain.

The example here uses a parallelization in which the analysis step is computed using the first model task and the same domain decomposition as the model. Other parallel configurations are possible. Although fully parallel execution of the assimilation program is highly efficient, it is constrained by the maximum job size permitted on the computer. The model used in the example here can scale even further than the 64 processes used for WRF. Hence, on the same computer, one could either execute a larger ensemble with fewer processes per model, resulting in a longer runtime, or opt for a smaller ensemble, which would reduce the runtime. The number of processes should be set so that the requirements for the ensemble size for a successful assimilation can be fulfilled. The other aspect is the required memory. The analysis step needs the whole ensemble stored in a domain-decomposed way. Thus, the complete ensemble is collected on the processes

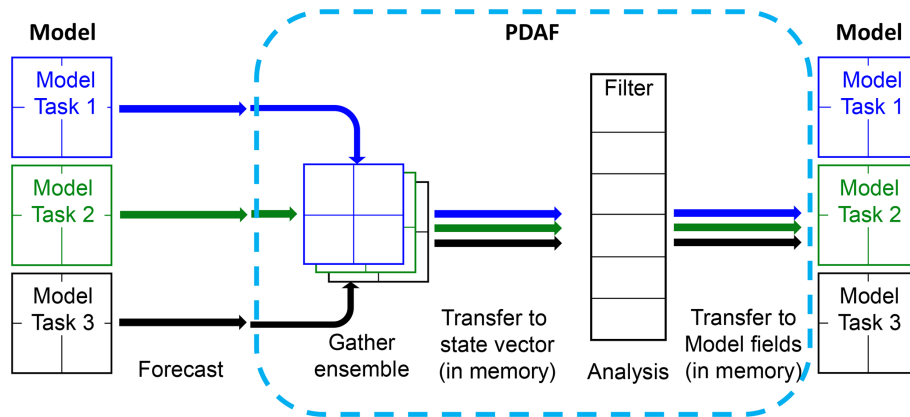


**Figure 6.** Diagram of data exchange between the model and PDAF in online mode.

of task 1, which calculate the analysis step. In extreme cases this might overload the available memory. For larger applications, one might need to obtain a compute allocation at larger computing sites, such as national compute centers.

In conclusion, this study elucidates the DA program by enhancing the WRF model code and employing in-memory data transfers between the model and PDAF. The Observation Module Infrastructure (OMI) plays a pivotal role in handling observational data, encompassing observation initialization, observation operators, and observation localization. While the current implementation includes operators for profile data ( $T$ ,  $U$ , and  $V$ ) and GNSS data (PW and ZTD), it maintains flexibility for incorporating complex remote sensing observation operators. The exemplary outcomes of perfect twin experiments affirm the effectiveness of the WRF-PDAF system in assimilating observations. Importantly, given that real-world forecasting times may be longer than ideal case scenarios operational DA performance could be even more efficient. Overall, the online WRF-PDAF system provides an efficient and promising framework for implementing high-resolution mesoscale forecasting and re-analysis, bridging the gap between cutting-edge research and practical applications in weather forecasting and climatology.

**Code availability.** Code can be downloaded at <https://doi.org/10.5281/zenodo.8367112> (Shao, 2023a).

**Data availability.** The dataset can be downloaded at <https://doi.org/10.5281/zenodo.10083810> (Shao, 2023b).

**Author contributions.** CS and LN planned the campaign. CS performed the experiments, analyzed the data, and wrote the paper draft. LN reviewed and edited the paper.

**Competing interests.** The contact author has declared that neither of the authors has any competing interests.

**Disclaimer.** Publisher's note: Copernicus Publications remains neutral with regard to jurisdictional claims made in the text, published maps, institutional affiliations, or any other geographical representation in this paper. While Copernicus Publications makes every effort to include appropriate place names, the final responsibility lies with the authors.

**Acknowledgements.** The calculations for this research were conducted on the high-performance computer of the Alfred Wagner Institute.

**Financial support.** Changliang Shao was supported by the China Scholarship Council for 1 year of research at AWI (no. 202105330044).

The article processing charges for this open-access publication were covered by the Alfred-Wegener-Institut Helmholtz-Zentrum für Polar- und Meeresforschung.

**Review statement.** This paper was edited by Yuefei Zeng and reviewed by two anonymous referees.

## References

- Anderson, J. L., Hoar, T., Raeder, K., Liu, H., Collins, N., Torn R., and Arellano, A.: The Data Assimilation Research Testbed: A Community Facility, *B. Am. Meteorol. Soc.*, 90, 1283–1296, <https://doi.org/10.1175/2009BAMS2618.1>, 2009.
- Bannister, R. N.: A review of operational methods of variational and ensemble-variational data assimilation, *Q. J. Roy. Meteor. Soc.*, 143, 607–633, <https://doi.org/10.1002/qj.2982>, 2017.

- Barker, D., Huang, X.-Y., Liu, Z., Auligné, T., Zhang, X., Rugg, S., Ajjaji, R., Bourgeois, A., Bray, J., Chen, Y., Demirtas, M., Guo, Y.-R., Henderson, T., Huang, W., Lin, H.-C., Michalakes, J., Rizvi, S., and Zhang, X.: The Weather Research and Forecasting Model's Community Variational/Ensemble Data Assimilation System: WRFDA, *B. Am. Meteorol. Soc.*, 93, 831–843, <https://doi.org/10.1175/BAMS-D-11-00167.1>, 2012.
- Brusdal, K., Brankart, J. M., Halberstadt, G., Evensen, G., Brasseur, P., van Leeuwen, P. J., Dombrowsky, E., and Veron, J.: A demonstration of ensemble-based assimilation methods with a layered ogcm from the perspective of operational ocean forecasting system, *J. Marine Syst.*, 40–41, 253–289, [https://doi.org/10.1016/S0924-7963\(03\)00021-6](https://doi.org/10.1016/S0924-7963(03)00021-6), 2003.
- Chandra, R., Dagum, L., Kohr, D., Menon, R., Maydan, D., and McDonald, J.: *Parallel programming in OpenMP*, Morgan Kaufmann, ISBN 9781558606718, 2001.
- Desroziers, G., Berre, L., Chapnik, B., and Poli, P.: Diagnosis of observation, background and analysis-error statistics in observation space, *Q. J. Roy. Meteor. Soc.*, 131, 3385–3396, <https://doi.org/10.1256/qj.05.108>, 2005.
- Feng, C. and Pu, Z.: The impacts of assimilating Aeolus horizontal line-of-sight winds on numerical predictions of Hurricane Ida (2021) and a mesoscale convective system over the Atlantic Ocean, *Atmos. Meas. Tech.*, 16, 2691–2708, <https://doi.org/10.5194/amt-16-2691-2023>, 2023.
- Gaspari, G. and Cohn, S. E.: Construction of Correlation Functions in Two and Three Dimensions, *Q. J. Roy. Meteor. Soc.*, 125, 723–757, <https://doi.org/10.1002/qj.4971255417>, 1999.
- Goodliff, M., Bruening, T., Schwichtenberg, F., Li, X., Lindenthal, A., Lorkowski, I., and Nerger, L.: Temperature assimilation into a coastal ocean-biogeochemical model: Assessment of weakly- and strongly-coupled data assimilation, *Ocean Dynam.*, 69, 1217–1237, <https://doi.org/10.1007/s10236-019-01299-7>, 2019.
- Greybush, S. J., Kalnay, E., Miyoshi, T., Ide, K., and Hunt, B. R.: Balance and Ensemble Kalman Filter Localization Techniques, *Mon. Weather Rev.*, 139, 511–522, <https://doi.org/10.1175/2010MWR3328.1>, 2011.
- Gropp, W., Lusk, E., and Skjellum, A.: *Using MPI: Portable Parallel Programming with the Message-Passing Interface*, The MIT Press, Cambridge, Massachusetts, ISBN 9780262571043, 1994.
- Holbach, H. M., Bousquet, O., Bucci, L., Chang, P., Cione, J., Ditchek, S., Doyle, J., Duvel, J.-P., Elston, J., Goni, G., Hon, K. K., Ito, K., Jelenak, Z., Lei, X., Lumpkin, R., McMahon, C. R., Reason, C., Sanabia, E., Shay, L. K., Sippel, J. A., Sushko, A., Tang, J., Tsuboki, K., Yamada, H., Zawislak, J., and Zhang, J. A.: Recent Advancements in Aircraft and In Situ Observations of Tropical Cyclones, *Tropical Cyclone Research and Review*, 12, 81–99, <https://doi.org/10.1016/j.tcr.2023.06.001>, 2023.
- Huang, B., Wang, X., Kleist, D. T., and Lei, T. A.: Simultaneous Multiscale Data Assimilation Using Scale-Dependent Localization in GSI-Based Hybrid 4D-EnVar for NCEP FV3-Based GFS, *Mon. Weather Rev.*, 2, 149, <https://doi.org/10.1175/MWR-D-20-0166.1>, 2021.
- Hunt, B. R., Kostelich, E. J. and Szunyogh, I.: Efficient data assimilation for spatiotemporal chaos: a local ensemble transform Kalman filter, *Physica D*, 230, 112–126, <https://doi.org/10.1016/j.physd.2006.11.008>, 2007.
- Karspeck, A. R., Danabasoglu, G., Anderson, J., Karol, S., Karol, S., Collins, N., Vertenstein, M., Raeder, K., Hoar, T., Neale, R., Edwards, J., and Craig, A.: A global coupled ensemble data assimilation system using the community earth system model and the data assimilation research testbed, *Q. J. Roy. Meteor. Soc.*, 144, 2304–2430, <https://doi.org/10.1002/qj.3308>, 2018.
- Kleist, D. T., Parrish, D. F., Derber, J. C., Treadon, R., Wu, W.-S., and Lord, S.: Introduction of the GSI into the NCEP Global Data Assimilation System, *Mon. Weather Rev.*, 24, 1691–1705, <https://doi.org/10.1175/2009WAF2222201.1>, 2009.
- Kurzrock, F., Nguyen, H., Sauer, J., Chane Ming, F., Cros, S., Smith Jr., W. L., Minnis, P., Palikonda, R., Jones, T. A., Lallemand, C., Linguet, L., and Lajoie, G.: Evaluation of WRF-DART (ARW v3.9.1.1 and DART Manhattan release) multiphase cloud water path assimilation for short-term solar irradiance forecasting in a tropical environment, *Geosci. Model Dev.*, 12, 3939–3954, <https://doi.org/10.5194/gmd-12-3939-2019>, 2019.
- Lawrence, B. N., Reznay, M., Budich, R., Bauer, P., Behrens, J., Carter, M., Deconinck, W., Ford, R., Maynard, C., Mullerworth, S., Osuna, C., Porter, A., Serradell, K., Valcke, S., Wedi, N., and Wilson, S.: Crossing the chasm: how to develop weather and climate models for next generation computers?, *Geosci. Model Dev.*, 11, 1799–1821, <https://doi.org/10.5194/gmd-11-1799-2018>, 2018.
- Li, L., Žagar, N., Raeder, K., and Anderson, J. L.: Comparison of temperature and wind observations in the Tropics in a perfect-model, global EnKF data assimilation system, *Q. J. Roy. Meteor. Soc.*, 149, 1–19, <https://doi.org/10.1002/qj.4511>, 2023.
- Li, Y., Cong, Z., and Yang, D.: Remotely Sensed Soil Moisture Assimilation in the Distributed Hydrological Model Based on the Error Subspace Transform Kalman Filter, *Remote Sens.*, 15, 1852, <https://doi.org/10.3390/rs15071852>, 2023.
- Liu, Y. A., Sun, Z., Chen, M., et al.: Assimilation of atmospheric infrared sounder radiances with WRF-GSI for improving typhoon forecast, *Front. Earth Sci.*, 12, 457–467, <https://doi.org/10.1007/s11707-018-0728-6>, 2018.
- Liu, Z., Ban, J., Hong, J.-S., and Kuo, Y.-H.: Multi-resolution incremental 4D-Var for WRF: Implementation and application at convective scale, *Q. J. Roy. Meteor. Soc.*, 146, 3661–3674, <https://doi.org/10.1002/qj.3865>, 2020.
- Lorenc, A. C.: Analysis methods for numerical weather prediction, *Q. J. Roy. Meteor. Soc.*, 112, 473, 1177–1194, <https://doi.org/10.1002/qj.49711247414>, 1986.
- Mingari, L., Folch, A., Prata, A. T., Pardini, F., Macedonio, G., and Costa, A.: Data assimilation of volcanic aerosol observations using FALL3D+PDAF, *Atmos. Chem. Phys.*, 22, 1773–1792, <https://doi.org/10.5194/acp-22-1773-2022>, 2022.
- Mu, L., Nerger, L., Streffingl, J., Tang, Q., Niraulal, B., Zampieri, L., Loza, S. N., and Goessling, H. F.: Sea-ice forecasts with an upgraded AWI Coupled Prediction System, *J. Adv. Model. Earth Sy.*, 14, e2021MS002631, <https://doi.org/10.1029/2022MS003176>, 2023.
- Nerger, L.: Data assimilation for nonlinear systems with a hybrid nonlinear Kalman ensemble transform filter, *Q. J. Roy. Meteor. Soc.*, 148, 620–640, <https://doi.org/10.1002/qj.4221>, 2022.
- Nerger, L. and Hiller, W.: Software for Ensemble-based Data Assimilation Systems-Implementation Strategies and Scalability, *Comput. Geosci.*, 55, 110–118, <https://doi.org/10.1016/j.cageo.2012.03.026>, 2013.
- Nerger, L., Danilov, S., Hiller, W., and Schröter, J.: Using sea-level data to constrain a finite-element primitive-equation ocean

- model with a local SEIK filter, *Ocean Dynam.*, 56, 634–649, <https://doi.org/10.1007/s10236-006-0083-0>, 2006.
- Nerger, L., Janjic, T., Schroeter, J., and Hiller, W.: A unification of ensemble square root filters, *Mon. Weather Rev.*, 140, 2335–2345, <https://doi.org/10.1175/MWR-D-11-00102.1>, 2012.
- Nerger, L., Tang, Q., and Mu, L.: Efficient ensemble data assimilation for coupled models with the Parallel Data Assimilation Framework: example of AWI-CM (AWI-CM-PDAF 1.0), *Geosci. Model Dev.*, 13, 4305–4321, <https://doi.org/10.5194/gmd-13-4305-2020>, 2020.
- OpenMP: OpenMP Application Program Interface Version 3.0, <http://www.openmp.org/> (last access: 26 June 2023), 2008.
- Pena, I. I.: Improving Satellite-Based Convective Storm Observations: An Operational Policy Based on Static Historical Data, Doctoral dissertation, Stevens Institute of Technology, ISBN 9798379567484, 2023.
- Pham, D. T., Verron, J., and Roubaud, M. C.: A singular evolutive extended Kalman filter for data assimilation in oceanography, *J. Marine Syst.*, 16, 323–340, [https://doi.org/10.1016/S0924-7963\(97\)00109-7](https://doi.org/10.1016/S0924-7963(97)00109-7), 1998.
- Raju, A., Parekh, A., Chowdary, J. S., and Gnanaseelan, C.: Impact of satellite-retrieved atmospheric temperature profiles assimilation on Asian summer monsoon 2010 simulation, *Theor. Appl. Climatol.*, 116, 317–326, <https://doi.org/10.1007/s00704-013-0956-3>, 2014.
- Rakesh, V., Singh, R., and Joshi, P. C.: Intercomparison of the performance of MMS/WRF with and without satellite data assimilation in short-range forecast applications over the Indian region, *Meteorol. Atmos. Phys.*, 105, 133–155, <https://doi.org/10.1007/s00703-009-0038-3>, 2009.
- Risanto, C. B., Castro, C. L., Arellano, A. F., Moker, J. M., and Adams, D. K.: The Impact of Assimilating GPS Precipitable Water Vapor in Convective-Permitting WRF-ARW on North American Monsoon Precipitation Forecasts over Northwest Mexico, *Mon. Weather Rev.*, 149, 3013–3035, <https://doi.org/10.1175/MWR-D-20-0394.1>, 2021.
- Shao, C.: shchl1/WRF-PDAF-development: v1.0 (v1.0), Zenodo [code], <https://doi.org/10.5281/zenodo.8367112>, 2023a.
- Shao, C.: shchl1/GMD-DATA: Data for GMD-WRF-PDAF\_V1.0 (v1.0.0), Zenodo [data set], <https://doi.org/10.5281/zenodo.10083810>, 2023b.
- Shao, C. and Nerger, L.: The Impact of Profiles Data Assimilation on an Ideal Tropical Cyclone Case, *Remote Sens.*, 16, 430, <https://doi.org/10.3390/rs16020430>, 2024.
- Skamarock, W. C., Klemp, J. B., Dudhia, J., Gill, D. O., Liu, Z., Berner, J., Wang, W., Powers, J. G., Duda, M. G., Barker, D., and Huang, X.: A Description of the Advanced Research WRF Model Version 4.3 (No. NCAR/TN-556+STR), <https://doi.org/10.5065/1dfh-6p97>, 2021.
- Song, L., Shen, F., Shao, C., Shu, A., and Zhu, L.: Impacts of 3D-EnVar-Based FY-3D MWS-2 Radiance Assimilation on Numerical Simulations of Landfalling Typhoon Ampil (2018), *Remote Sens.*, 14, 6037, <https://doi.org/10.3390/rs14236037>, 2022.
- Sun, J., Jiang, Y., Zhang, S., Zhang, W., Lu, L., Liu, G., Chen, Y., Xing, X., Lin, X., and Wu, L.: An online ensemble coupled data assimilation capability for the Community Earth System Model: system design and evaluation, *Geosci. Model Dev.*, 15, 4805–4830, <https://doi.org/10.5194/gmd-15-4805-2022>, 2022.
- Tödter, J. and Ahrens, B.: A second-order exact ensemble square root filter for nonlinear data assimilation, *Mon. Weather Rev.*, 143, 1347–1467, <https://doi.org/10.1175/MWR-D-14-00108.1>, 2015.
- Wang, Q., Danilov, S., and Schröter, J.: Finite element ocean circulation model based on triangular prismatic elements with application in studying the effect of topography representation, *J. Geophys. Res.*, 113, C05015, <https://doi.org/10.1029/2007JC004482>, 2008.
- Wang, S. and Qiao, X.: A local data assimilation method (Local DA v1.0) and its application in a simulated typhoon case, *Geosci. Model Dev.*, 15, 8869–8897, <https://doi.org/10.5194/gmd-15-8869-2022>, 2022.
- Xue, M., Droegemeier, K., and Wong, V.: The Advanced Regional Prediction System (ARPS) – A multi-scale nonhydrostatic atmospheric simulation and prediction model. Part I: Model dynamics and verification, *Meteorol. Atmos. Phys.*, 75, 161–193, <https://doi.org/10.1007/s007030070003>, 2000.
- Yang, Y., Wang, Y., and Zhu, K.: Assimilation of Chinese Doppler Radar and Lightning Data Using WRF-GSI: A Case Study of Mesoscale Convective System, *Adv. Meteorol.*, 2015, 763919, <https://doi.org/10.1155/2015/763919>, 2015.
- Zhang, S., Harrison, M. J., Rosati, A., and Wittenberg, A.: System Design and Evaluation of Coupled Ensemble Data Assimilation for Global Oceanic Climate Studies, *Mon. Weather Rev.*, 135, 3541–3564, <https://doi.org/10.1175/MWR3466.1>, 2007.
- Zheng, Y., Albergel, C., Munier, S., Bonan, B., and Calvet, J.-C.: An offline framework for high-dimensional ensemble Kalman filters to reduce the time to solution, *Geosci. Model Dev.*, 13, 3607–3625, <https://doi.org/10.5194/gmd-13-3607-2020>, 2020.
- Zupanski, D., Zhang, S. Q., Zupanski, M., Hou, A. Y., and Cheung, S. H.: A Prototype WRF-Based Ensemble Data Assimilation System for Dynamically Downscaling Satellite Precipitation Observations, *J. Hydrometeorol.*, 12, 118–134, <https://doi.org/10.1175/2010JHM1271.1>, 2011.